*Proc. Indian Acad. Sci.* (*Chem. Sci.*), Vol. 113, No. 1, February 2001, pp 63–76


# An insight into the passivation of cupronickel alloys in chloride environment

J MATHIYARASU, N PALANISWAMY and V S MURALIDHARAN*
Corrosion Science and Engineering Division, Central Electrochemical Research Institute, Karaikudi 630 006, India
e-mail: corr@cscecri.ren.nic.in

MS received 19 August 2000; revised 2 December 2000

**Abstract.** Cupronickels offer enhanced corrosion protection in marine environments by the formation of passive films on the surface. Cyclic voltammetric studies were carried on cupronickels in chloride solutions at *p*H 6·3 to understand the role of chloride ions in passive film formation. Increase in nickel content of the alloy and of chloride ions in solution decreases film resistance. Chloride ions take part in reduction of the passive film to copper. A solid-state model for passive film formation involving chloride ions has been attempted.

**Keywords.** Cupronickels; passivation; solid-state model; cyclic voltammetry; marine environment.

## 1. Introduction

Cupronickels are widely used in chloride environments due to their marked corrosion resistance. The corrosion resistance of these alloys is due to passivation, which occurs at a critical electron-to-atom ratio of copper and nickel at which the *d* shell becomes unfilled [1,2]. The passivation in chloride solutions is due to a protective oxide layer. In synthetic seawater, the layer is found to contain $Cu_2O$, $Cu_2(OH)_3Cl$ while in NaCl solutions the layer dissolves to form soluble $CuCl_2^-$ complexes [3]. Nickel dissolves to form its corrosion products because of its greater solubility. The dissolution of copper results in the formation of an outer $Cu_2(OH)_3Cl$ layer with an inner $Cu_2O$ layer [4–7]. In synthetic seawater, the film formed on 90/10 cupronickels contains mainly $Cu_2O$ with a small amount of $Ni^{2+}$, $Ni^{3+}$ and chloride ions in the inner layer [8]. This $Cu_2O$ film grows till the potential of the outer film surface reaches that of $Cu_2(OH)_3Cl$. After sometime, the inner layer stops growing and a non-protective porous outer layer of $Cu_2(OH)_3Cl$ is formed [9–10].

Cupronickel alloys containing up to 40 wt% nickel are particularly interesting since it has been shown that corrosion rates decrease with increasing nickel content from 10 to 40% and then remain constant [11]. Films formed on the alloys containing more than 40 wt% of copper (if the atomic ratio of Cu/Ni exceeds 1.6) are less stable [12]. In low chloride solutions, a nickel-rich alloy undergoes pitting while in higher chloride solutions passivation takes place. Interesting behaviour of Cu–Ni alloys is observed in the presence of chloride ions, where passive layers formed on these materials suffer localised break-down. Various authors attempted to understand the effect of chloride ion concentration

*For correspondence

on the passivation behaviour of cupronickels. A critical chloride concentration, below which the resistance to localised corrosion increases with decreasing nickel content and also above which it increases with nickel content has been reported [13]. The present investigation focuses on the role of chloride ions in the formation of passive films on cupronickels with varying nickel content. A solid-state model has also been attempted.

## 2. Experimental details

Different cupronickel alloys were made from pure metals in inert atmosphere, and then mechanically treated and heat-treated to obtain void-free single-phase materials. Compositions of the alloys used in this study are given in table 1. The alloys were made into cylindrical rods having area of cross-section = 0·385 $cm^2$. The rods were embedded in teflon gaskets and electrically connected by screw and thread arrangements. The rods were mechanically polished with 1/0, 2/0, 3/0 and 4/0 emery papers. Three-electrode cell assemblies were used. Large platinum foils were used as auxiliary electrodes and

**Table 1.** Compositions (wt%) of experimental cupronickel alloys used as working electrodes.

| Cupronickels | Copper % | Nickel % |
|---|---|---|
| Alloy A | 85 | 15 |
| Alloy B | 73 | 27 |
| Alloy C | 65 | 35 |

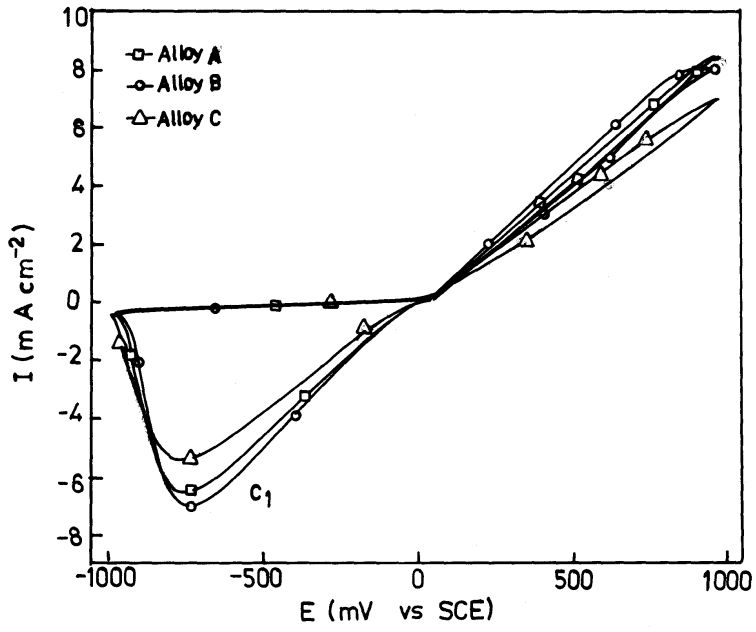


**Figure 1.** Cyclic voltammograms of cupronickel alloys in 0·02 M chloride solution at 10 mV/s sweep rate, $e_{l,c}$ = –1·0 V, $e_{l,a}$ = 1·0 V.

saturated calomel electrodes as reference. Triangular potential sweep experiments were carried out using an electrochemical analyser BAS 100 A. Voltammograms were obtained from –1000 mV to 1000 mV at various sweep rates (5–100 mV/s) in 0·02<*x*> 0·5 M sodium chloride solutions at *p*H 6·3. After cycling between 0 to 600 mV, the surface of the alloy C was seen under scanning electron microscope at different magnifications.

X-ray diffraction studies of the film formed on the alloy surface were carried out by using a computer-controlled X-diffractometer (JOEL 8030) with $CuK_{\mu}$ radiation ($l$ = 1·5418 Å) at a rating of 40 kV, 20 mA. The scan rate was 0·05 per step and the measuring time was one second per step.

XPS studies were carried out using ESCA-Lab 2000 (VG scientific instruments) and the surface was sputtered as required by argon ion bombardments. A delocalised $Ar^+$ ion beam accelerated under 2 keV was used to remove adsorbed contaminants on the surface (0·05 $\mu/m^2$ current density). The excitation source used was the unmonochromatised Al $K_{\mu}$ ($hg$ = 1486·6 eV). The spectra were recorded at a vacuum better than $7{\cdot}1 \times 10^{-7}$ $N/m^2$.

SEM micrographs of electrodes polarized at different anodic potentials were obtained to correlate the electrochemical and surface morphological data. A scanning electron microscope model HITACHI-S 3000H was used.

## 3. Results

### 3.1 *Behaviour of cupronickels in different chloride concentrations*

3.1a *Electrochemical behaviour in 0·02 M chloride solutions:* When polarised from –1000 to 1000 mV, the forward scan exhibited no peak in all the cupronickel alloys studied. In the case of alloy C, the reverse scan showed a cathodic peak at –774 mV which became more negative with sweep rates. When the nickel content was reduced to 20%, the alloy exhibited a cathodic peak at –658 mV; on further decrease of nickel content to 10%, the reverse scan showed cathodic peaks at –662 mV and –512 mV which became active with sweep rates (figure 1).

3.1b *Electrochemical behaviour in 0·05 M chloride solutions:* When polarised from –1000 to 1000 mV, the forward scan exhibited an anodic peak at 539 mV followed by oxygen evolution for alloy C. The reverse scan revealed an inverted anodic peak at 458 mV followed by a well-defined cathodic peak at –555 mV. In the case of alloy B, the anodic peak appeared at 469 mV, while the cathodic peak was at –471 mV. When the nickel percentage in the alloy was reduced to 10%, the anodic peak was not observed during the forward scan while the reverse scan showed two cathodic peaks at –662 mV and –512 mV (figure 2).

3.1c *Electrochemical behaviour in 0·1 M chloride solutions:* During the forward scan of alloy C, an anodic peak appeared at 372 mV which became nobler with sweep rate; the reverse scan exhibited an inverted anodic peak at 235 mV and a cathodic peak at –417 mV. Alloy B exhibited a shoulder around 609 mV preceded by an anodic peak at 310 mV. The reverse scan exhibited a broad cathodic peak at –373 mV which became active with sweep rate. During the forward scan alloy A exhibited a shoulder at 234 mV followed by oxygen evolution. The reverse scan exhibited a peak at –383 mV which became active with sweep rate (figure 3).

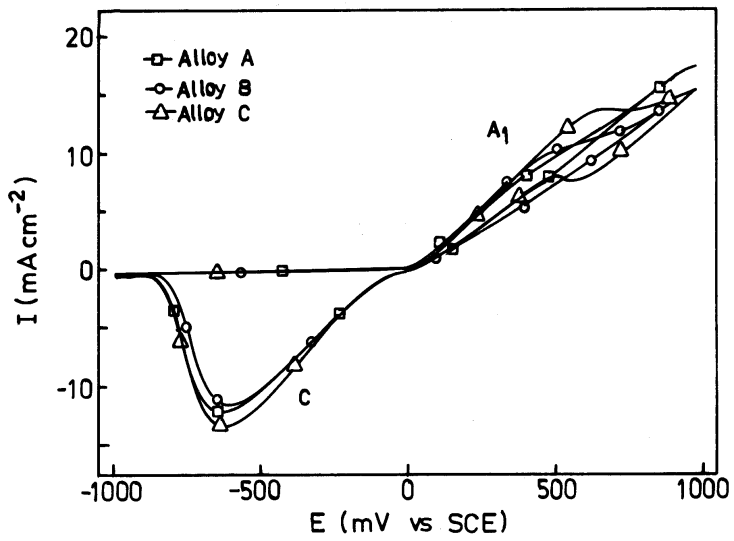


**Figure 2.** Cyclic voltammograms of cupronickel alloys in 0·05 M chloride solution at 10 mV/s sweep rate, $e_{l,c}$ = –1·0 V, $e_{l,a}$ = 1·0 V.

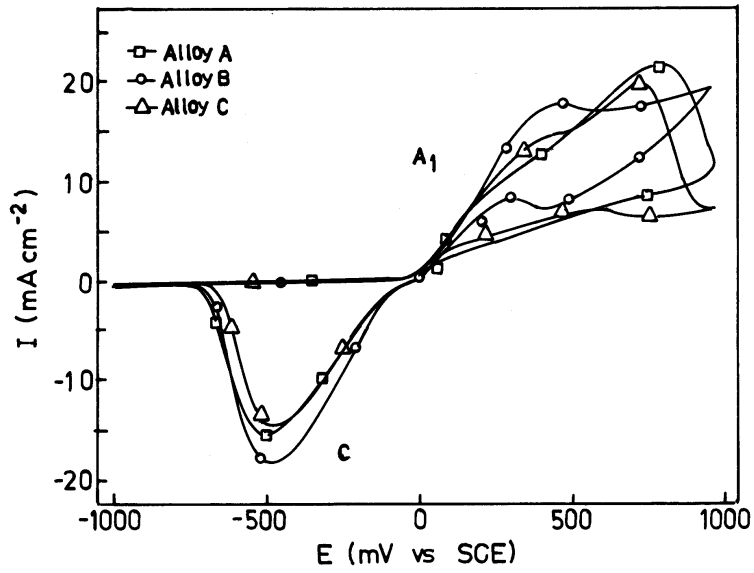


**Figure 3.** Cyclic voltammograms of cupronickel alloys in 0·01 M chloride solution at 10 mV/s sweep rate, $e_{l,c}$ = –1·0 V, $e_{l,a}$ = 1·0 V.

3.1d *Electrochemical behaviour in 0·2 M chloride solutions:* When polarised from –1000 to 1000 mV, the forward scan exhibited an anodic peak at 298 mV and the cathodic peak at –354 mV for alloy C. Two anodic peaks were observed at 191 mV and

467 mV for alloy B and these potentials became nobler with sweep rate. The reverse scan exhibited an inverted anodic peak at 133 mV followed by a cathodic peak at 294 mV. Similar behaviour was observed for alloy A. The forward scan exhibited anodic peaks at 143 mV and 446 mV and an inverted anodic peak at 330 mV followed by a cathodic peak at –283 mV in the reverse scan (figure 4).

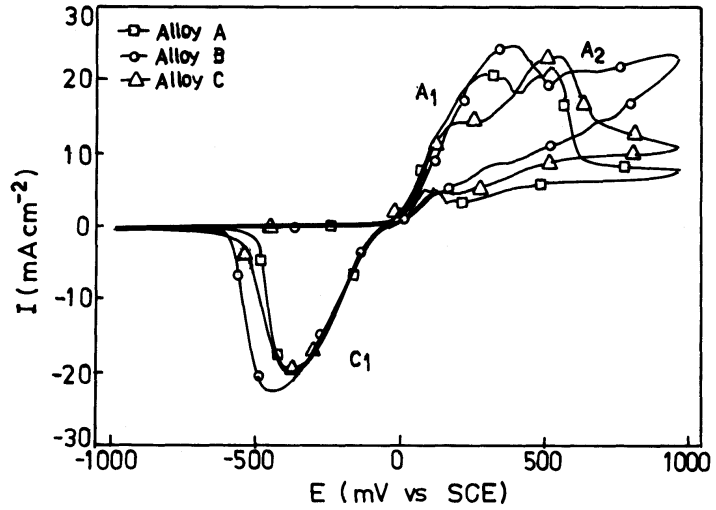


**Figure 4.** Cyclic voltammograms of cupronickel alloys in 0·2 M chloride solution at 10 mV/s sweep rate, $e_{l,c}$ = –1·0 V, $e_{l,a}$ = 1·0 V.

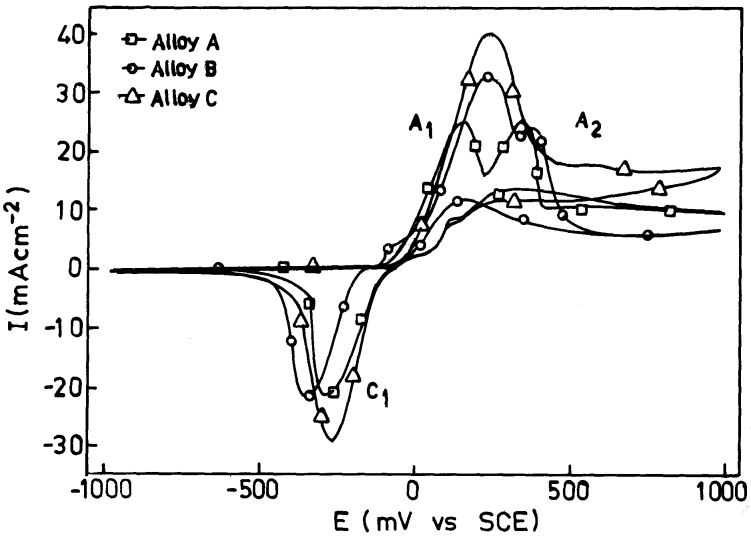


**Figure 5.** Cyclic voltammograms of cupronickel alloys in 0·5 M chloride solution at 10 mV/s sweep rate, $e_{l,c}$ = –1·0 V, $e_{l,a}$ = 1·0 V.

3.1e *Electrochemical behaviour in 0·5 M chloride solutions:* During the forward scan, alloy C exhibited a single anodic peak at 150 mV, and an inverted shoulder at 10 mV followed by a cathodic peak at –230 mV. Alloy B exhibited a sharp anodic peak at 130 mV followed by another peak at 270 mV. The reverse scan revealed a large inverted broad anodic peak at 180 mV, while the inverted shoulder became a distinct plateau at –30 mV; the cathodic peak appeared at –190 mV. When the nickel content in the alloy was 10%, an anodic peak was seen at 90 mV followed by a peak at 200 mV. In the reverse scan an inverted shoulder appeared at –60 mV; a distinct cathodic peak also appeared at –200 mV (figure 5).

### 3.2 *X-ray diffraction analysis*

Figure 6 presents the XRD patterns obtained for alloy C, at + 200 mV in 0·5 M solutions. The surface is found to have $Cu_3Ni_8$ as suggested by the *d*-spacing values of 2·079, 1·799 and 1·267. Oxidation of copper resulting in $Cu_2O$ is inferred by the *d*-spacing values of 2·469, 2·137 and 1·511.

### 3.3 *ESCA analysis*

The alloy C was maintained at desired potentials to identify the oxidation states of elements present underneath the surface film. The chemical compounds present in the passive film were determined from the detailed examination of oxidation states of elements present.

Figures 7 and 8 show the ESCA survey spectra (0–1000 eV) obtained from the surface exposed at various anodic potentials. The surface contamination was removed by etching the surface with $Ar^+$ ions. The survey scans indicated that the main elements in the film were Cu, O, C and traces of chloride and nickel. With increasing potential the signals corresponding to metallic copper and nickel decreased and contributions of signals at higher binding energies grew due to the formation of oxides and hydroxides. The surface kept at –200 mV, revealed the lack of shake-up satellite for both 2*P*3/2 and 2*P*1/2 suggesting the existence of elemental copper to be in the metallic form or in the cuprous form. No appreciable signal from the nickel couple was obtained at –200 mV. At 0 mV, the appearance of Cu.2*P*3/2 peak with satellites suggested that the copper might be

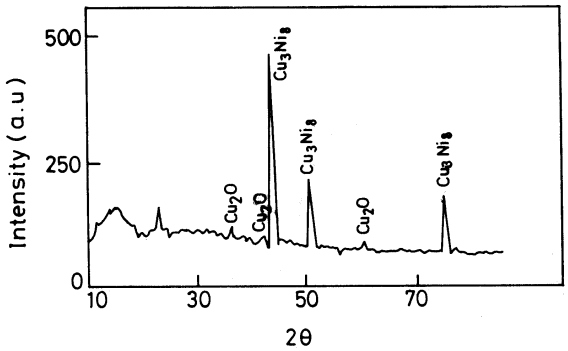


**Figure 6.** XRD pattern of alloy C kept at +200 mV.

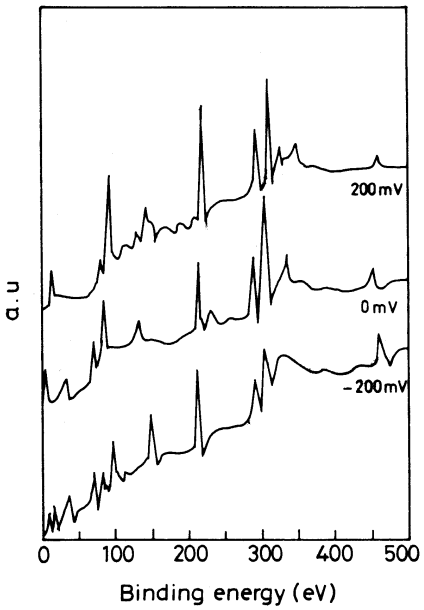


**Figure 7.** ESCA survey spectra (0–500 eV) of alloy C kept at various anodic potentials.

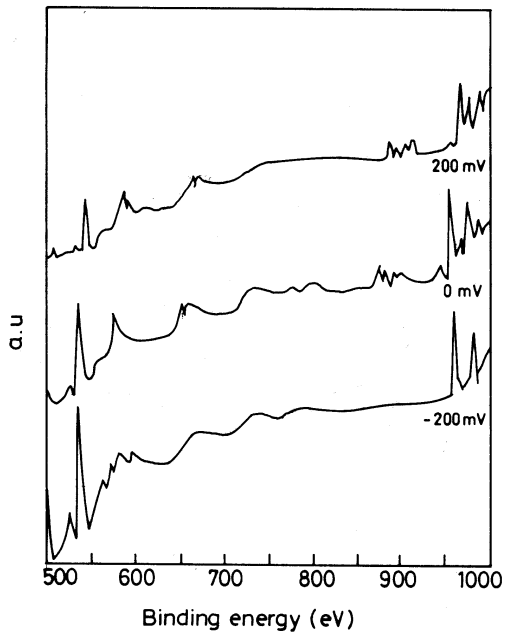


**Figure 8.** ESCA survey spectra (500–1000 eV) of alloy C kept at various anodic potentials.

present in the cuprous form. The $O_{1s}$ peak was asymmetric at all potentials with a maximum of 537 eV with a higher binding energy shoulder at 533 eV. The relative shift in the 1*s* peak and the appearance of the shoulder clearly indicated the presence of oxygen in the oxide–metal (O–M peak) binding state. The electrode kept at 200 mV exhibited the presence of satellite structure in addition to the 2*P*3/2 peak, corresponding to the divalent copper in addition to the monovalent copper. The relative shift between the 2*P*3/2 and 2*P*1/2 was found to be 20 eV instead of 19·8 eV (for pure copper) confirming the presence of CuO in the surface film. The spectra of copper compound established that the shake-up satellite structure was closely related to the oxidation state of copper. The 2*p* spectra of the cupric compounds showed satellite peaks arising from multi-electron excitation accompanying X-ray induced photo ionization.

## 4. Discussion

In the case of alloy dissolution [14] one would expect (a) both copper and nickel to leave the metal lattice, and/or (b) copper to dissolve and enter the solution.

In all chloride solutions studied, anodic and cathodic peak potentials varied with chloride ion concentration. At concentrations > 0·05 M, alloys A and B showed two distinct anodic peaks $A_1$ and $A_2$ in the forward scan. The appearance of peak $A_1$ is due to the formation of $Cu_2O$ via $CuCl_2^-$ which is an intermediate [15,16],

$$Cu + 2Cl^- \rightarrow CuCl_2^- + e, \tag{1}$$

$$2CuCl_2^- + H_2O \rightarrow Cu_2O + 4Cl^- + 2H^+. \tag{2}$$

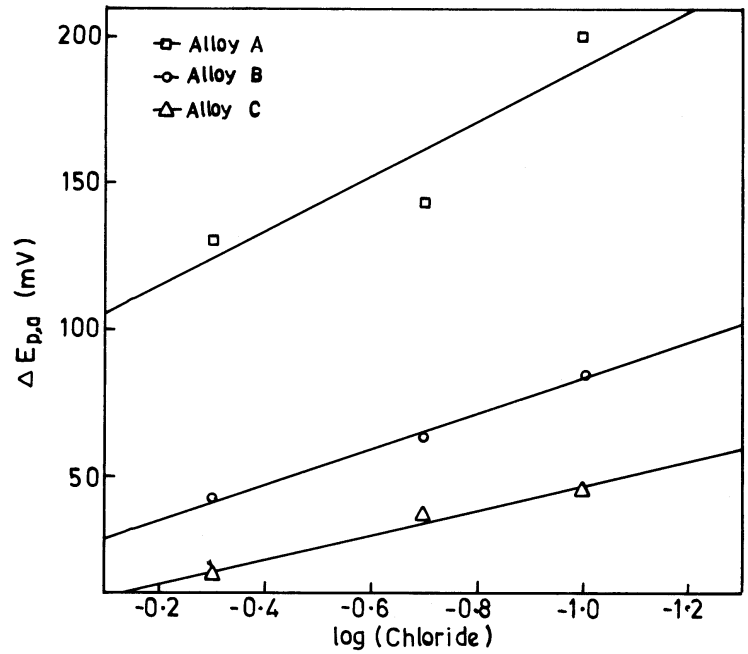


**Figure 9.** Peak potential separation ($\Delta E_p$) vs log chloride concentration for various cupronickel alloys.

At extreme anodic potentials the appearance of peak $A_2$ suggests that $Cu_2O$ would be oxidised to $CuO/Cu(OH)_2$.

$$Cu_2O + H_2O \rightarrow 2CuO + 2H^+, \tag{3}$$

$$Cu_2O + 3H_2O \rightarrow 2Cu(OH)_2 + 2H^+. \tag{4}$$

The Nernst equation for (1) is,

$$E_e = E_e^o + 2{\cdot}303RT/F \log [CuCl_2^-]/[Cu]\,[Cl^-]^2, \tag{5}$$

$$\Delta E_p = E_{p,a} - E_{p,c} = \text{peak potential separation}$$

$$= (E_{p,c} - E_e) - (E_{p,a} - E_e)$$

$$= 2{\cdot}303RT/F \log [CuCl_2^-]/[Cu]\,[Cl^-]^2. \tag{6}$$

The $CuCl_2^-$ undergoes chemical reaction to form $Cu_2O$. This suggests chloride ion participation in film formation. Figure 9 presents the peak potential separation ($\Delta E_p$) with log chloride ion concentration which confirms this. Scanning electron microscope picture (figure 10a) obtained on alloy C, when viewed at 1000 magnification, suggests the coverage of the surface by massive, voluminous, interconnecting crystals; on further magnification (figure 10b), rhombic and cubic crystals were seen. The surface of the base alloy was also seen. The base alloy substrate was covered completely after prolonged anodic polarisation.

An increase of chloride ion concentration in solution and copper content in the alloy caused the appearance of inverted anodic peaks, a net flow of anodic current. These suggest a predominant dissolution of the less noble component in the alloy through the pores of the passive film formed on the surface of the alloy (figure 10c).

The model for passivation was proposed by Muller [17,18], and describes the growth of the film only at certain points on the alloy and extends over the surface as a layer of uniform thickness ($d$). This film formation is controlled by Ohmic resistance. If the total area of the electrode is $A_o$ and $qp$ is the degree of coverage of the electrode, the resistance of the solution in the pores threading the layer is,

$$R_p = d/KA_o\,(1-q_p), \tag{7}$$

where $d$ is the thickness of the film and $K$ is the specific conductivity of the solution inside the pores. The expressions for peak current and peak potential are

$$i_{p,a} = ((nFrK)^{1/2}/M^{1/2})\,A_o\,(1-q_p)v^{1/2}, \tag{8}$$

$$E_{p,a} = E_o + ((nFrK)^{1/2}/M^{1/2})\{(d/K) + R_oA(1-q_p)\}v^{1/2}, \tag{9}$$

where $n$ = number of electrons involved in the electrochemical reaction, $r$ = film density; and $R_o$ is the resistance of the solution external to the film. As suggested by the above equations the anodic peak current reaches zero as the sweep rate tends to zero. Anodic peak ($A_1$) potentials were extrapolated to zero sweep rates (figure 11). The intersection

potential $E_a^o$ is the minimum potential needed for current flow, i.e. film formation potential. The decrease in copper content in the alloy shifts the $E_a^o$ to nobler values suggesting an hindrance to the film formation. Chloride ion concentration favours the film formation as indicated by the shift of $E_a^o$ to less noble values (table 2).

Monovalent copper film formation occurs at peak potential $A_1$. The surface coverage $q_p$ after the peak $A_1$ was calculated assuming the $r$ of $Cu_2O$ as 6·0 g/cc; $M$ = molecular weight of $Cu_2O$ = 143·09 g/mol; $K = 10^{-2}$ ohm$^{-1}$ cm$^{-1}$ in the preceding equations.

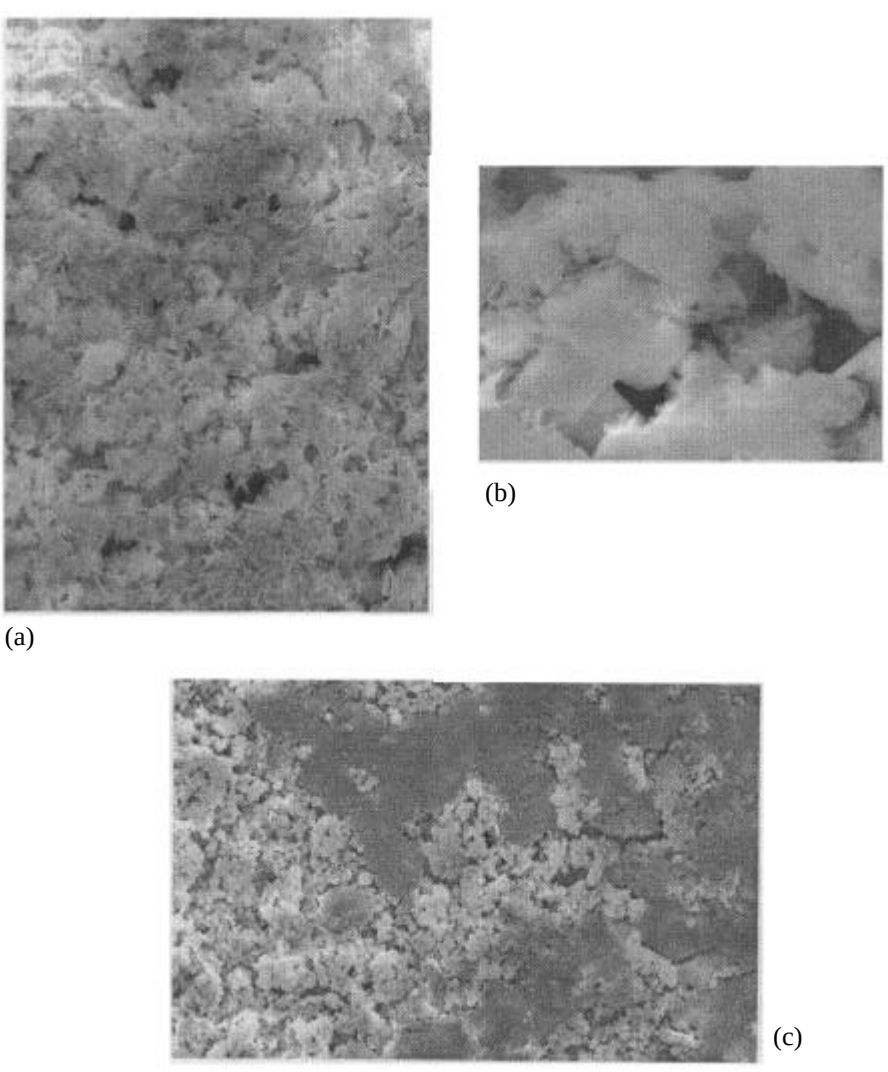


**Figure 10.** Scanning electron micrograph of alloy C, obtained by scanning the electrode potential from –200 to 600 mV vs SCE at 10 mV/s in 0·5 M NaCl (**a**) × 1000; (**b**) × 7000; (**c**) × 350.

**Table 2.** Variation of $E_a^o$ (mV vs SCE) with chloride ion concentration for different cupronickel alloys.

| Concentration of chloride (M) | Alloy A | Alloy B | Alloy C |
|---|---|---|---|
| 0·1 | 220 | 270 | 290 |
| 0·2 | 130 | 150 | 200 |
| 0·5 | –10 | 5 | 25 |

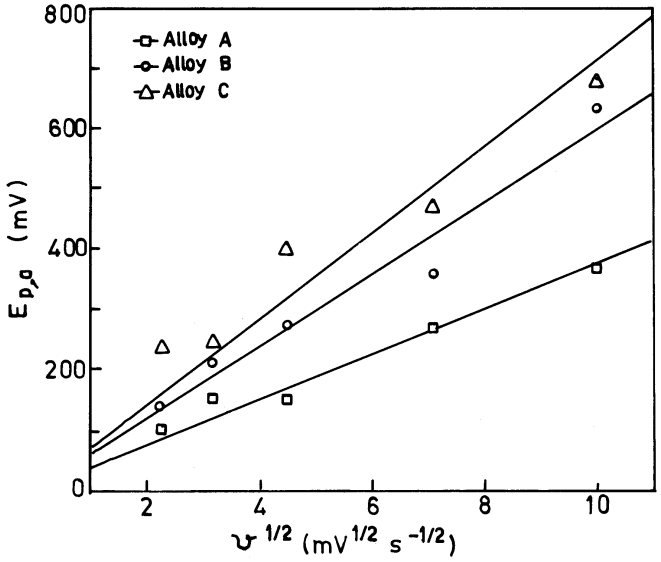


**Figure 11.** Anodic peak potential vs square root of sweep rates for various cupronickel alloys in 0·5 M chloride solutions.

The thickness of the film *d*, and the ohmic resistance *R* of the film were calculated.

The rise in chloride ion concentration did not affect markedly the film thickness (figure 12) while the film resistance decreased for all the alloys (figure 13). $Cu_2O$ film growth was invariant with chloride ions while its conductance was affected by them.

## 5. Solid-state passivation model

When cupronickel is subjected to prolonged anodic polarisation the dissolution of copper may give rise to $CuCl_2^-$ which in turn becomes $Cu_2O$. The alloy surface is covered by the film. The copper ion concentration within the film thickness decreases gradually. The migration of monovalent copper ions away from the alloy surface generates cation vacancies [19] as

$$Cu_{Cu}\,(ox) \rightarrow Cu^+(aq.) + V'_{Cu}\,(ox), \tag{10}$$

where $Cu_{Cu}$ (ox) is a monovalent copper ion site inside the film; $V'_{Cu}$ (ox) is vacancy of copper ions.

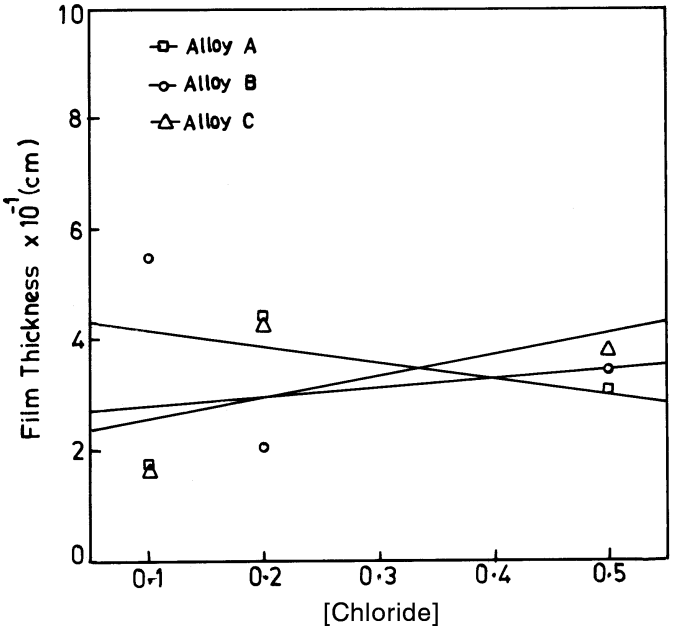


**Figure 12.** Film thickness (*d*) vs chloride concentration for various cupronickel alloys.

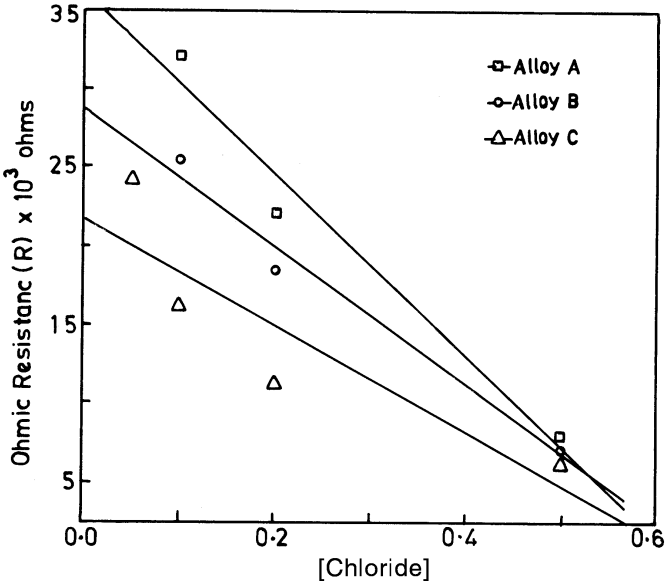


**Figure 13.** Ohmic resistance (*R*) vs chloride concentration for various cupronickel alloys.

When the electrode is made anodic, the cations move away from the electrode while cation vacancies travel towards it,

$$Cu_{Cu}\,(M) + V'_{Cu}\ (ox) \rightarrow Cu_{Cu}\,(ox) + V_{cu}\,(M) + e, \quad (11)$$

where $Cu_{Cu}$ (M) is the cationic site in the alloy, $V_{cu}$ (M) is the vacancy created by the copper cation in the alloy.

When nickel dissolution potential is reached, $Ni^{2+}$ ions try to occupy the cation vacancies,

$$Ni_{Ni}\,(M) + V'_{Cu}\ (ox) \rightarrow Ni_{Cu}\,(ox) + 2e, \quad (12)$$

where $Ni_{Cu}$ (ox) is the site where nickel divalent cation occupies the vacancy created by copper in the oxide. With the passage of time, outward diffusion of nickel ions occurs from the alloy/film interface to the inside of the film. This generates additional cation vacancies in the alloy. As the formation of soluble $NiCl_2$ is more favourable than that of $CuCl_2$, nickel ions leave faster from the oxide layer, which in turn generates further vacancies in the film,

$$Ni_{Cu}V_{Cu} \rightarrow Ni^{2+}\,(aq.) + 2\,V'_{Cu}\ (ox). \quad (13)$$

Chloride ions adsorb on the surface of the film and try to occupy the vacancies created by the oxygen ions of $Cu_2O$ [20–23]. The inward diffusion from the solution/film interface inside the film is facilitated by anodic polarization,

$$V_O\,(ox) + Cl^- \rightarrow Cl_O\,(ox). \quad (14)$$

As the chloride ion incorporation in the film increases, the number of oxygen vacancies occupied by chloride ions also increases. Chemical stability is decided by the copper and chloride ions ratio in this film. When the atomic ratio of $Cu^+$:$Cl^-$ exceeds 1, the film becomes unstable and dissolution occurs from the areas where the chloride ion concentration is greater (see figure 10c).

## 6. Conclusions

In chloride solutions cupronickels form $Cu_2O$ films on anodic polarisation. Chloride ions adsorb on the surface and occupy the oxygen vacancies in the film. Nickel content in the alloy and chloride ion concentration in solution decrease the resistance of $Cu_2O$ films. Nickel ions generate cation vacancies in the film when the conditions of $NiCl_2$ formation are favoured. The Cu:$Cl^-$ ion ratio in the film of $Cu_2O$ decides the chemical stability of $Cu_2O$ and if the ratio exceeds one, dissolution of oxide occurs.

## Acknowledgement

One of the authors (JM) expresses his sincere thanks to the Council of Scientific & Industrial Research, New Delhi for a fellowship.

## References

1. Uhlig H H 1944 *Trans. Electrochem. Soc.* **85** 307
2. Uhlig H H 1958 *Z. Electrochem.* **62** 700

3. Dhar H P, White R E, Darby R, Cornwell L R, Griffin R B and Burnwell G 1985 *Corrosion* **41** 193
4. Beccaria A M and Crousier J 1989 *Br. Corros. J*. **24** 49
5. Popplewell J M, Hart R J and Forrd J A 1973 *Corros. Sci*. **13** 295
6. North R F and Pryor M J 1968 *Corros. Sci*. **8** 149
7. Shih H and Pickering H W 1987 *J. Electrochem. Soc.* **134** 1949
8. Chauhan P K and Gadiyar H S 1985 *Corros. Sci.* **25** 55
9. Eiseltein L E, Syrett B C, Wing S S and Caligiuri R D 1983 *Corros. Sci.* **23** 223
10. Mathiyarasu J, Palaniswamy N and Muralidharan V S 1999 *Port. Electrochim. Acta* **17** 45
11. LaQue F L 1941 *J. Am. Nav. Eng*. **53** 9
12. Mansfeld F and Uhlig H H 1969 *Corros. Sci*. **9** 377
13. Milosev I and Metikos-Hukovic M 1997 *Electrochim. Acta* **42** 1537
14. Lee H P and Nobe K 1985 *J. Electrochem. Soc.* **132** 1031
15. Milosev I and Metikos-Hukovic M 1991 *J. Electrochem. Soc.* **138** 61
16. Pickering H W and Wagner C 1967 *J. Electrochem. Soc.* **114** 698
17. Muller W J 1931 *Trans. Faraday Soc*. **27** 737
18. Muralidharan V S, Thangavel K and Rajagopalan K S 1983 *Electrochim. Acta* **23** 1611
19. Urquidi M and Macdonald D D 1985 *J. Electrochem. Soc*. **132** 555
20. Urquidi-Macdonald M and Macdonald D D 1989 *J. Electrochem. Soc*. **136** 961
21. Chao C Y, Lin L F and Macdonald D D 1981 *J. Electrochem. Soc*. **128** 1187
22. Lin L F, Chao C Y and Macdonald D D 1981 *J. Electrochem. Soc*. **128** 1194
23. Macdonald D D, Ben-Haim D D and Pallix J 1989 *J. Electrochem. Soc*. **136** 3269